Journal of Alloys and Compounds 499 (2010) 200–205

Contents lists available at ScienceDirect

Journal of Alloys and Compounds

journal homepage: www.elsevier.com/locate/jallcom

Ultrafine Al_2O_3–B_4C composites consolidated by pulsed electric current sintering

A.K. Swarnakar, S.G. Huang, O. Van der Biest, J. Vleugels *

Department of Metallurgy and Materials Engineering, K.U. Leuven, Kasteelpark Arenberg 44, B-3001 Leuven, Belgium

ARTICLE INFO

Article history:
Received 19 November 2009
Received in revised form 17 March 2010
Accepted 18 March 2010
Available online 25 March 2010

Keywords:
Ceramic composite
Sintering
Microstructure
Pulsed electric current sintering

ABSTRACT

Al_2O_3–60 vol.% B_4C composites with 0–5 wt% SiC addition were consolidated by pulsed electric current sintering (PECS) during 4 min at 1650 °C. The influence of the SiC additive on the densification behaviour, microstructure and mechanical properties of the Al_2O_3–B_4C composites were investigated. Microstructural analysis revealed the presence of $Al_{18}B_4O_{33}$ grains, formed by chemical reaction of Al_2O_3 with surface oxides on B_4C, in agreement with thermodynamic calculations. The Al_2O_3 grains were found to coarsen from 0.22 μm in the starting powder up to about 0.60 μm during PECS, whereas the size of the ~0.6 μm B_4C grains hardly changed. The Al_2O_3 and B_4C grain size slightly decreased upon SiC addition. The addition of 3 or 5 wt% SiC hardly influenced the hardness and toughness of the Al_2O_3–B_4C composites, whereas the strength and stiffness were reduced. The composite with 1 wt% SiC combined a hardness of 26 GPa, an *E*-modulus of 448 GPa, a bending strength of 600 MPa and a fracture toughness of 6.2 MPa $m^{1/2}$. The influence of the loading condition and dwell time during PECS of the 5 wt% SiC doped composite was assessed.

1. Introduction

Monolithic alumina (Al_2O_3) ceramics are used in many fields due to the unique combination of strength, hardness, thermal resistance and electrical insulation. However, the low fracture toughness is limiting the application as structural component [1,2]. Boron carbide (B_4C) exhibits many attractive properties such as low density, high melting point and high hardness, which makes it suitable for light-duty armour, high-temperature structural parts, cutting tools, wear parts and thermo-mechanical applications. Moreover, B_4C has a good wear resistance and high-temperature hardness compared to other carbides, which makes it suitable for wear applications [3,4]. Full densification of undoped B_4C however is a challenge. Recent developments on B_4C-based composites are focused on reducing the densification temperature either by using sintering additives or the use of alternative sintering technologies to achieve higher fracture toughness and strength [5,6]. PECS densification of B_4C composites with TiC and Al_2O_3 was reported to be feasible at lower temperatures compared to hot pressing [4,7]. Moreover, a small amount of Al_2O_3 was found to improve the relative density of B_4C to a large extent and B_4C composites with 10 wt% Al_2O_3 could be densified by PECS at 1900 °C for 2 min [7]. TiB_2 addition to B_4C has been reported to result in a higher fracture toughness [6]. The addition of TiC, TiB_2, WC or SiC particles in an Al_2O_3 matrix improve the fracture toughness, hardness, and strength for cutting tool applications [8–12]. The mechanical properties of Al_2O_3 were successfully improved with addition of 5–20 vol.% of whisker like and shardlike shaped B_4C particles [13]. Moreover, small amounts of SiC were found to significantly improve the strength of Al_2O_3-based ceramics [11,12,14–19]. In accordance with the scarce information on sintering and characterization B_4C–Al_2O_3 composites [20], no information is available on the properties of SiC doped Al_2O_3–B_4C composites. It is well recognized that both microstructural refinement and full densification of the final product are desirable in many powder based material systems.

In the present study, the effect of small amounts of SiC addition on the densification behaviour, microstructure and mechanical properties of Al_2O_3–60 vol.% B_4C was investigated. The ceramic composites were densified by pulsed electric current sintering (PECS), also known as spark plasma sintering (SPS). This sintering technique has the advantage of higher heating rates and shorter dwell times in comparison with conventional hot pressing [21,22]. Higher densities, refined microstructures, clean grain boundaries and elimination of surface impurities, as well as an overall improvement in materials performance are reported for PECS densified ceramics [22–24].

Since sintering is carried out in a closed graphite die/punch set-up, some in situ generated gas or volatile phases might be trapped inside the powder compact during sintering. Thin oxide layers, i.e. B_2O_3 compounds, are always present on the surface of B_4C starting powders. Therefore, it is also important to investigate the influence of different PECS loading cycles on the densification and final microstructure of the SiC doped Al_2O_3–B_4C composites.

* Corresponding author. Tel.: +32 16 321244; fax: +32 16 321992.
E-mail address: Jozef.Vleugels@mtm.kuleuven.be (J. Vleugels).

0925-8388/$ – see front matter © 2010 Elsevier B.V. All rights reserved.
doi:10.1016/j.jallcom.2010.03.166

2. Experimental procedures

Commercially available B_4C (Grade AS974, ESK, 0.6 μm), α-Al_2O_3 (TM-DAR, Taimicron, 0.22 μm), and β-SiC (grade HSC-059, Superior Graphite, USA, 0.7 μm) powders were used as starting materials for the SiC doped Al_2O_3–B_4C composites. Composites with 60 vol.% B_4C and 0 wt% (AB60), 1 wt% (AB60S1), 3 wt% (AB60S3) and 5 wt% (AB60S5) SiC additions were wet-mixed in ethanol on a multidirectional mixer (Turbula T2A, WAB, Switzerland) using alumina-milling balls (ϕ = 10 mm, grade AL9, Cerlim, France) for 48 h. After mixing, the suspensions were dried on a rotating evaporator at 65 °C and granulated through a 315 μm sieve.

The composite powders were pulsed electric current sintered (PECS, Type HP D25/1, FCT Systeme, Rauenstein, Germany) under a maximum pressure of 80 MPa in a 30 mm graphite die for 4 min at 1650 °C. The initial heating rate was 200 °C/min up to 1050 °C and 100 °C/min up to 1650 °C. The uniaxial pressure was gradually increased from 8 to 40 MPa in the 400–1050 °C region and increased to 80 MPa during the 0.5 min dwell period at 1050 °C, as further indicated as thermal cycle TC1. The PECS process is a rather fast sintering procedure but homogenization of the temperature distribution is an important issue, especially when sintering electrically insulating or poorly conductive materials. Therefore, a dwell period of 0.5 min is incorporated at 1050 °C. Horizontal and vertical graphite foils were used to separate the graphite die/punch set-up from the powder compact. To minimize the heat loss by thermal radiation, a porous carbon felt (Sigratherm flexible carbon felt, SGC carbon group, Wiesbaden, Germany) insulation was placed around the graphite die. Details on the equipment, the die/punch set-up and temperature measurement are provided elsewhere [25,26].

After PECS and sand-blasting, the cross-sectioned samples were polished up to 1 μm diamond paste. The bulk density of the composites was measured by the Archimedes method in ethanol. The microstructure was examined by scanning electron microscopy (SEM, XL30-FEG, FEI, Eindhoven, The Netherlands), equipped with an energy dispersive analysis system (EDS, EDAX, Tilburg, The Netherlands) for compositional analysis. The average Al_2O_3 and B_4C grain size was determined from SEM micrographs using Image-pro Plus software [27] to measure the linear intercept length of at least 100 grains for each material grade. The Vickers hardness (HV_5), was measured (Model FV-700, Future-Tech Corp., Tokyo, Japan) with an indentation load of 49.05 N. The fracture toughness, K_{IC}, was calculated from the length of the cracks of the Vickers indentations according to the formula of Shetty et al. [28] and Niihara [29]. X-ray diffraction (XRD) patterns were recorded on a Seifert 3003 T/T, X-ray diffractometer using Cu Kα radiation. The elastic modulus of the ceramics was measured according to the resonance frequency method, as measured by the impulse excitation technique (Model Grindo-Sonic, J.W. Lemmens N.V., Leuven, Belgium). The sample surfaces for *E*-modulus and strength testing were ground with a diamond grinding wheel (type D46SW-50-X2, Technodiamant, The Netherlands) on a Jung grinding machine (JF415DS, Göppingen, Germany). The 3-point flexural strength was measured on rectangular samples (25 mm × 3 mm × 2 mm), with a span length of 20 mm and a cross-head displacement of 0.1 mm/min.

3. Results and discussion

3.1. Densification behaviour

The in situ shrinkage curves of the Al_2O_3–B_4C powder compacts with and without 5 wt% SiC during PECS are compared in Fig. 1. Blank runs using the graphite die/punch set-up without powder were performed to extract the densification curves from the experimentally registered piston travel during PECS. No substantial densification was observed below 1050 °C under a maximum pressure of 40 MPa. All composite grades however started to shrink rapidly during the heating stage from 1050 to 1650 °C under a pressure of 80 MPa. The onset of densification of B_4C without additives during PECS was reported to be at 1500 °C whereas maximum densification was achieved at 1900 °C [5]. Therefore, the shrinkage peak between 1050 and 1235 °C can be attributed to the densification of Al_2O_3 grains. The displacement of the undoped Al_2O_3–B_4C composite levels off after 2 min at 1650 °C, whereas that of the 5 wt% SiC doped composite gradually increases during the dwell period of 4 min, implying that a longer dwell time is needed to fully densify the higher SiC content composite.

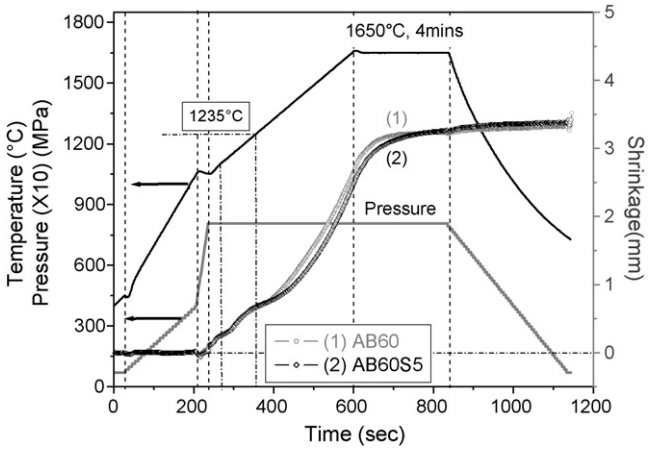

Fig. 1. Representative densification behaviour of undoped and 5 wt% SiC doped Al_2O_3–60 vol.% B_4C composites during PECS according to the thermal cycle TC1 (1650 °C with 4 min dwell time at 80 MPa).

The bulk and relative density of the Al_2O_3–B_4C composites sintered for 4 min at 1650 °C are summarized in Table 1. The theoretical density (TD) of the composites was calculated according to the rule of mixtures, using a theoretical density of 3.94, 2.52 and 3.16 g/cm^3 for Al_2O_3, B_4C and SiC respectively. Although the relative density does not take into account potential reaction products or solid solutions, the data in Table 1 indicate that the final density of the Al_2O_3–B_4C composites apparently decreases with increasing SiC content. SEM analysis of cross-sectioned polished samples revealed the presence of a small amount of residual porosity, especially in the 5 wt% SiC doped grades. The observed amount however is substantially smaller than the relative density calculations indicate.

The present experimental results revealed that Al_2O_3-based composites with 60 vol.% B_4C with or without 1 wt% SiC addition can be nearly fully densified within 4 min at 1650 °C and 80 MPa. The total PECS thermal cycle only took 20 min, including heating and cooling, whereas 1 h at 1850 °C and 75 MPa was needed to densify Al_2O_3–40 vol.% B_4C composites by means of hot pressing [20].

The loading cycle can also influence the densification, especially when gasses are released during the thermal cycle. When applying the maximum load too early in the thermal cycle, these gasses might get trapped in the powder compact and inhibit densification, whereas vapour products can be easily removed from the sintering compact by the vacuum environment when delaying the load increase. Therefore, the densification behaviour of the Al_2O_3–B_4C powder compacts with 5 wt% SiC content was studied in more detail in two additional sintering cycles, shown in Fig. 2(a) and (b). In the second thermal cycle, TC2, the heating rate of 200 °C/min was maintained up to 1650 °C, whereas the pressure was gradually increased from the minimum up to 80 MPa during heating from

Table 1
Physical properties of the SiC doped Al_2O_3–60 vol.% B_4C composites PECS at 1650 °C under different processing cycles.

Grade	Thermal cycle	SiC (wt%)	ρ (g/cm^3)	R.D. (%)	*E* (GPa)	HV_5 (GPa)	$K_{IC(Shetty)}$ (MPa m$^{1/2}$)	$K_{IC(Anstis)}$ (MPa m$^{1/2}$)	TRS (MPa)
AB60	TC1	0	3.03	98.1	445	24.35 ± 0.50	5.6 ± 0.2	7.2 ± 0.3	596 ± 39
AB60S1	TC1	1	3.05	98.5	448	25.88 ± 0.98	6.2 ± 0.1	7.9 ± 0.3	580 ± 54
AB60S3	TC1	3	2.99	96.6	434	24.03 ± 0.98	5.6 ± 0.2	7.1 ± 0.2	488 ± 22
AB60S5	TC1	5	3.02	97.5	439	24.53 ± 0.65	5.7 ± 0.2	7.3 ± 0.2	506 ± 59
AB60S5	TC2	5	3.00	97.1	400	22.48 ± 0.94	4.5 ± 0.1	5.8 ± 0.1	–
AB60S5	TC3	5	2.94	95.1	380	22.70 ± 0.50	4.8 ± 0.3	6.1 ± 0.3	–

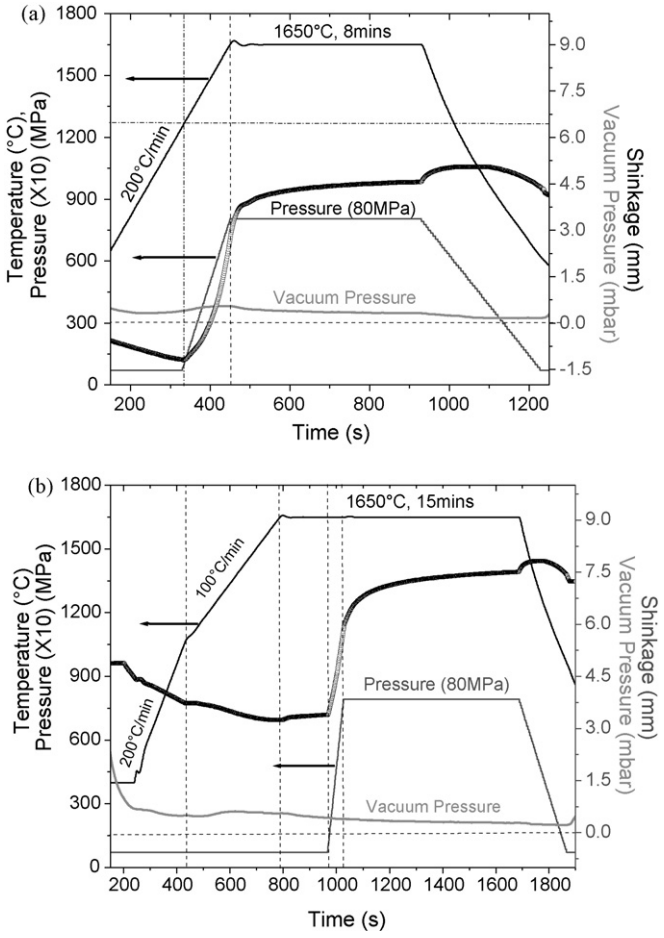

Fig. 2. Representative densification behaviour of Al_2O_3–60 vol.% B_4C with 5 wt% SiC doped composite during PECS according to the thermal cycle TC2 (a) (pressure applied at 1250 °C) and TC3 (b) (pressure applied at 1650 °C).

1250 to 1650 °C. Based on the punch displacement, i.e. shrinkage during the experiment, the dwell time was stopped after 8 min, as shown in Fig. 2a. The densification started upon increasing the pressure at 1250 °C, reaching a maximum shrinkage rate at 1650 °C. TC2 resulted in a composite density of 3.00 g/cm^3 (97% TD), which is similar as for TC1 (see Table 1).

In thermal cycle TC3, the initial heating rate of 200 °C/min was reduced to 100 °C/min in the 1050–1650 °C range, whereas the pressure was increased from the minimum up to 80 MPa after a 3 min dwell time at 1650 °C, as shown in Fig. 2b. The dwell period was stopped after 12 min when the densification levelled off, resulting in a final density of 2.94 g/cm^3 (95% TD). Again, the maximum densification rate was observed upon increasing the load but the obtained density is lower than in TC1 and TC2. This can be attributed to the longer dwell time at 1650 °C, providing more time for interphase reactions (see further) resulting in a lower apparent density of the ceramic. The shrinkage curve in TC2 and TC3 indicates the onset of densification upon increased pressure. The vacuum pressure during sintering is also plotted in Fig. 2(a) and (b), revealing no substantial gas evolution during thermal cycling.

3.2. Constituent phases

The room temperature XRD patterns of the ground Al_2O_3–B_4C composites are compared in Fig. 3. All composites contain mainly α-Al_2O_3 and rhombohedral B_4C. As expected, the peak intensity of SiC increases with increasing addition in the starting powder, implying that the SiC phase is chemically stable in the Al_2O_3–B_4C

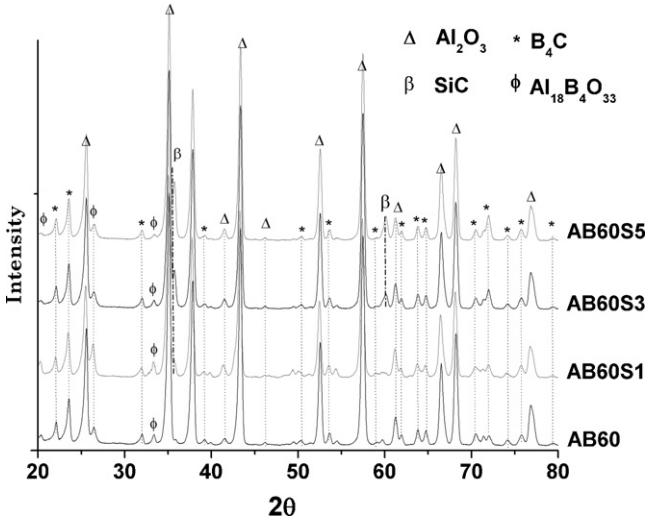

Fig. 3. XRD patterns of ground surfaces of Al_2O_3–B_4C–SiC composites, PECS according to thermal cycle TC1.

matrix. However, additional peaks that could be matched to the $Al_{18}B_4O_{33}$ ($9Al_2O_3{\cdot}2B_2O_3$) phase were detected in all composites.

The observation of a small amount of $Al_{18}B_4O_{33}$ in the sintered composites is consistent with the work of Wang et al. [30] on the combustion reaction of Al, B_2O_3 and C and the thermite reaction of Al and B_2O_3 in argon. The reaction product in a combusted 4 mol Al, 2 mol B_2O_3 and 1 mol C mixture was reported to contain mainly Al_2O_3, some B_4C and a small amount of Al_2O_3-rich borate, i.e., $Al_{18}B_4O_{33}$ formed according to reaction (1) [30]. According to Logan et al., $Al_{18}B_4O_{33}$ was observed when combusting Al–B_2O_3 both in air and argon [31]. $Al_{18}B_4O_{33}$ formation was also reported during self-propagation high-temperature synthesis of Al_2O_3/B_4C composites [32].

In the investigated Al_2O_3–B_4C system, the formation of $Al_{18}B_4O_{33}$ can be explained by a combination of reactions (1)–(3):

$$9Al_2O_3(s) + 2B_2O_3(g) \Leftrightarrow Al_{18}B_4O_{33}(s) \quad (1)$$

$$B_4C(s) + 4O_2(g) \Leftrightarrow 2B_2O_3(g) + CO_2(g) \quad (2)$$

$$B_4C(s) + 4O_2(g) + 9Al_2O_3(s) \Leftrightarrow Al_{18}B_4O_{33}(s) + CO_2(g) \quad (3)$$

$$B_4C(s) + 2.5Al_2O_3(s) \Leftrightarrow 2B_2O_2(g) + 2.5Al_2O(g) + CO(g) \quad (4)$$

The evolution of the Gibbs energy of these reactions with temperature, as calculated by FactSage software [33], is shown in Fig. 4,

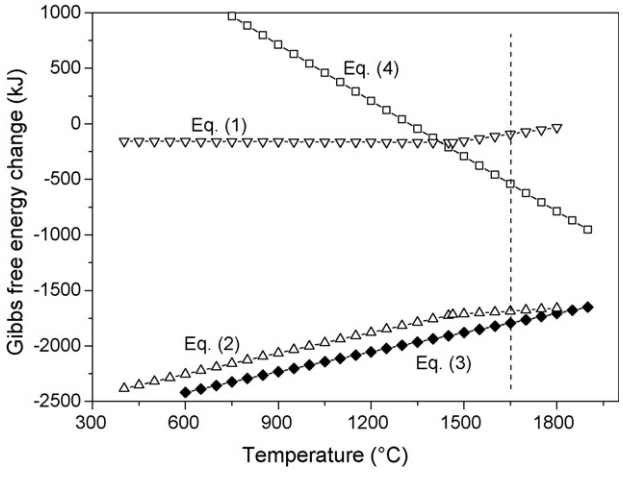

Fig. 4. Gibbs energy change of reactions (1)–(4) as a function of temperature.

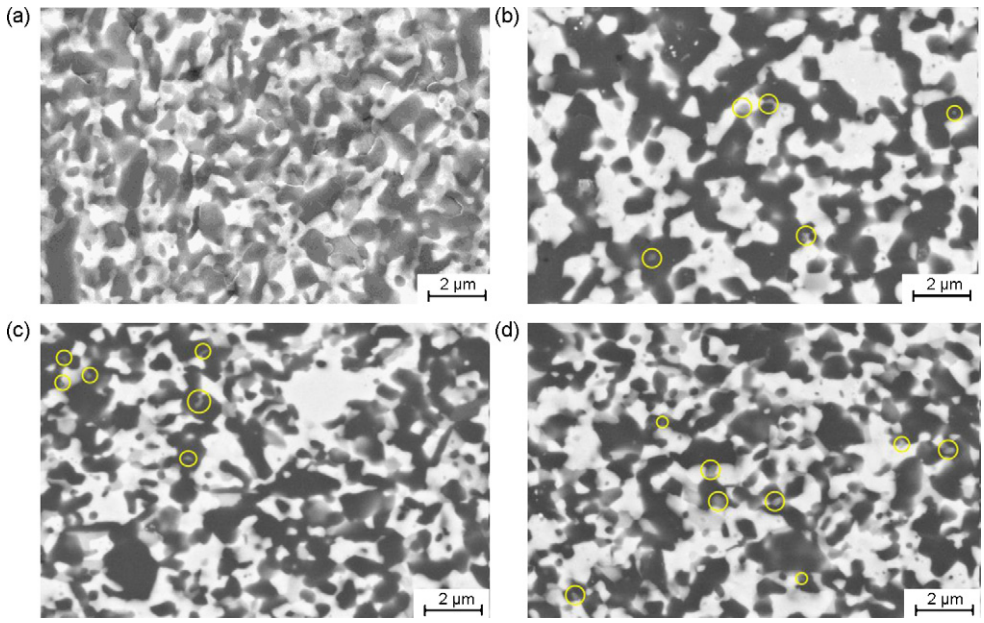

Fig. 5. Secondary electron micrographs of Al_2O_3–60 vol.% B_4C composites with 0 wt% (a), 1 wt% (b), 3 wt% (c) and 5 wt% (d) SiC, PECS at 1650 °C for 4 min according to the thermal cycle TC1. Some SiC grains are marked by circles.

revealing that reactions (2) and (3) are most favourable under standard conditions during thermal cycling up to 1650 °C. The oxidation of B_4C is thermodynamically favourable when B_4C is exposed to an O_2 atmosphere. Submicrometer B_4C powders were indeed found to slowly oxidise at room temperature in wet air forming a layer of B_2O_3, HBO_2 or H_3BO_3 [34]. At higher temperature, a B_2O_3 glass film was formed during oxidation of micrometer sized B_4C powders at 500 °C in air [35]. According to the specifications of the suppliers, the oxygen content in the B_4C starting powder was 2.1 wt%, implying a B_2O_3 film was already present on the B_4C starting powder. Since PECS was conducted in a vacuum of 100 Pa, it is expected that only a small amount of additional B_2O_3 was formed during thermal cycling. According to the Gibbs energy change of reaction (1), $Al_{18}B_4O_{33}$ will be formed under the applied experimental conditions, which is also consistent with the Al_2O_3–B_2O_3 phase diagram [36,37]. Although B_4C could also react directly with Al_2O_3 at 1650 °C according to reaction (4), the ΔG of −541 kJ at 1650 °C is substantially smaller than −1792 kJ for reaction (3). Furthermore, no substantial gas evolution was detected during PECS of the Al_2O_3–B_4C composites, indicating reaction (4) did not proceed.

The influence of the Al_2O_3/B_2O_3 ratio on the formation of $Al_4B_2O_9$ and $Al_{18}B_4O_{33}$ phases in the Al_2O_3–B_2O_3 phase diagram, as calculated by FactSage, was reported as a function of temperature, suggesting that the formation of crystalline $Al_{18}B_4O_{33}$ is possible by the reaction of amorphous B_2O_3 and Al_2O_3 at 1000 °C [37]. The reported theoretical density of 2.68 g/cm^3 of $Al_{18}B_4O_{33}$ [37] is lower than for Al_2O_3 and SiC, implying that the actual density of the PECS composites is higher than the calculated relative theoretical density suggests.

3.3. Microstructural analysis

Representative secondary electron micrographs of the composites with 0–5 wt% SiC, PECS according to thermal cycle TC1, are compared in Fig. 5. The dark and bright phases correspond to B_4C and Al_2O_3 respectively, whereas the grey contrast grains are either SiC or $Al_{18}B_4O_{33}$. The constituent phases were homogeneously distributed in all composites. The Al_2O_3 and B_4C grain size slightly decreased with increasing SiC content implying that SiC is not an efficient grain growth inhibitor for both phases. In the SiC-free grade, the average Al_2O_3 and B_4C grain size is 0.56 and 0.63 μm, whereas the grain size decreased to 0.56 and 0.52 μm respectively in the 5 wt% SiC grade. Monolithic Al_2O_3 can be PECS around 1200 °C and the average grain size increases rapidly with increasing sintering temperature [11,12]. The addition of nanometer sized SiC particles to an Al_2O_3 matrix however can reduce grain growth by grain boundary pinning [11]. Several researchers have studied the effect of SiC addition on the densification behaviour and microstructural properties of Al_2O_3/SiC composites [11,14–19]. SiC nanopowder addition was reported to delay densification and grain growth of an Al_2O_3 matrix providing the SiC particles is mainly located at intergranular positions [14]. Due to the relatively large size of the B_4C starting powder in this work, the B_4C grains are mainly present in direct contact with Al_2O_3 grains, at triple pockets or in contact with the $Al_{18}B_4O_{33}$ phase. The SiC grains pin the alumina grain boundaries, not only resulting in a reduced alumina grain size but also a reduced densification rate due to the limited grain boundary diffusivity at the Al_2O_3–SiC interface [15].

The SiC starting powder used in this study might be too large to be an efficient grain growth inhibitor. The fact that the size of the B_4C phase in the densified composites is comparable to that of the starting powder, i.e. 0.6 μm, whereas the alumina phase only coarsened from 0.22 up to 0.60 μm indicates that both phases already efficiently act as mutual grain growth inhibitors by grain boundary pinning.

Representative SEM micrographs of the 5 wt.% SiC doped Al_2O_3–B_4C composites PECS according to thermal cycle TC2 and TC3 are shown in Fig. 6, revealing that the longer dwell time and slower initial heating rate in TC3 leads to an increased grain size. The average grain size of the Al_2O_3, B_4C and SiC phases decreased from respectively 0.49, 0.78 and 0.65 μm after TC3 to 0.40, 0.71 and 0.59 μm after TC2.

3.4. Mechanical properties

The Young's modulus (E), Vickers hardness (HV_5) and fracture toughness (K_{IC}) of the PECS composites are compared in Table 1. The stiffness of the composites is nearly constant at different SiC contents. Upon the addition of 1 wt% SiC, the hardness of the Al_2O_3–B_4C composites increased from 24.35 to 25.88 GPa, what could be

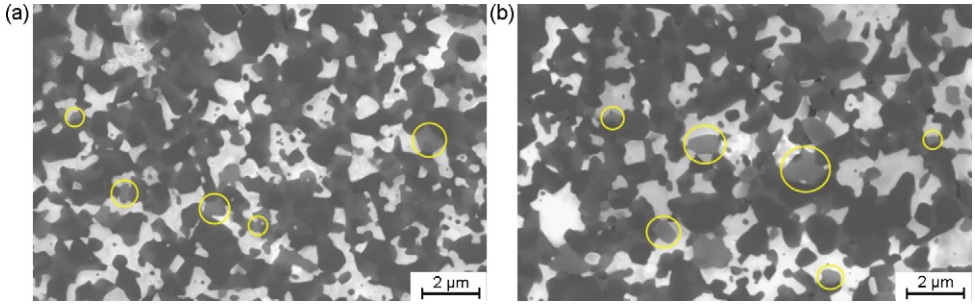

Fig. 6. SEM micrographs of 5 wt.% SiC doped Al_2O_3–60 vol.% B_4C composites, PECS at 1650 °C according to thermal cycle TC2 (a) and TC3 (b). Some SiC grains are marked by circles.

correlated with an improved densification, whereas the strength and toughness was comparable.

It should be mentioned that the way of calculating the fracture toughness is determined by the crack pattern, i.e., either according to a radial/median or Palmqvist crack mode. To identify the crack mode, the indented surfaces were additionally polished for a few minutes with 3 μm diamond paste. The original and repolished indentations are shown in Fig. 7(a)–(d). The gap in-between the edge of the polished indentation and the actual crack reveals a Palmqvist crack mode in the Al_2O_3–B_4C composites [38]. The indentation toughness can therefore be calculated according to the formula of Niihara [29] and Shetty et al. [28], as summarised in Table 1. A similar crack pattern was reported for undoped B_4C, PECS at 1900 °C, resulting in a toughness of 3.9–4.2 MPa $m^{1/2}$, as calculated according to both the Niihara and Shetty equation [39].

The toughness of the composites, PECS according to thermal cycle TC1, hardly changes as function of the SiC content. The Niihara and Shetty toughness was measured to be 5.6 and 7.2 MPa $m^{1/2}$ respectively, which is substantially higher than the 3.9–4.2 MPa $m^{1/2}$ for single phase B_4C material [39]. The toughness of the composites prepared according to TC2 and TC3 was lower.

Investigating the crack propagation of the Palmqvist cracks originating at the corners of Vickers indentations revealed that the cracks propagated both inter- and transgranularly in all PECS Al_2O_3–B_4C composites. Since the nature of the crack propagation is not influenced by the addition of SiC, the fracture toughness of the composites is comparable.

No improvement in hardness and toughness were measured at higher SiC contents of 3 and 5 wt%. Although the Al_2O_3 and B_4C grains were finer, the hardness was comparable and the strength and stiffness were slightly lower than for the undoped composite. This should be attributed to the higher residual porosity in these composites.

The *E*-modulus of the 5 wt% SiC doped ceramics decreased from 439 to 400 and 380 GPa after TC1, TC2 and TC3 respectively (see Table 1), indicating an increased interphase reactivity with the formation of $Al_{18}B_4O_{33}$ due to the increased dwell time at 1650 °C, rather than a decreased density. The presence of $Al_{18}B_4O_{33}$ was also reported to assist pressureless densification by liquid phase formation, but leads to poor mechanical properties [40].

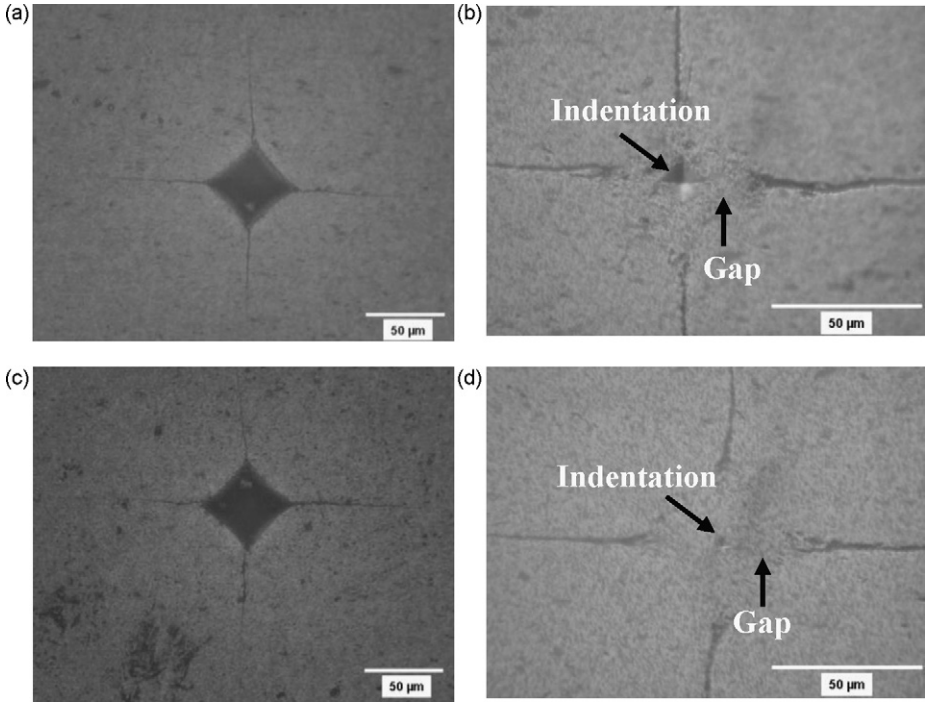

Fig. 7. Optical micrographs of 49 N Vickers indentions before (a and c) and after (b and d) additional polishing on Al_2O_3–60 vol.% B_4C composites without (a and b) and with (c and d) 5 wt% SiC, PECS according to thermal cycle TC1.

4. Conclusions

Near fully dense submicrometer sized Al_2O_3-based composites with 60 vol.% B_4C with or without 1 wt% SiC could be obtained within 20 min by means of pulsed electric current sintering at 1650 °C for 4 min under a pressure of 80 MPa. The average grain size of the Al_2O_3 and B_4C phase is 0.55 μm. Due to the partial oxidation of the B_4C phase, a small amount of $Al_{18}B_4O_{33}$ was formed during PECS. The addition of SiC delayed densification of the Al_2O_3–B_4C composites and hardly influenced the grain size of the B_4C and Al_2O_3 phases. The properties of the composite hardly changed by the addition of 1 wt % SiC resulting in a composite exhibiting a hardness of 26 GPa, an *E*-modulus of 448 GPa, a bending strength of 600 MPa and an acceptable toughness of 6.2 MPa $m^{1/2}$. The 3 and 5 wt% SiC doped composites were not fully densified after 4 min at 1650 °C and 80 MPa, resulting in slightly inferior properties.

The loading cycle influenced the material properties, whereas a longer dwell time up to 15 min at 1650 °C led to an increased but still submicrometer grain size of all phases. The mechanical properties like *E*-modulus, hardness, fracture toughness and overall density decreased with increasing dwell time at 1650 °C due to an increased amount of $Al_{18}B_4O_{33}$.

Acknowledgements

This work was performed within the framework of the Research Fund of K.U. Leuven under project GOA/08/007. The authors also acknowledge the Fund for Scientific Research Flanders under grant number G.0305.07.

References

[1] Y. Zhou, K. Hirao, Y. Yamauchi, S. Kanzaki, J. Eur. Ceram. Soc. 24 (2004) 3465–3470.
[2] K.H. Mina, S.T. Oh, Y.D. Kim, I.H. Moona, J. Alloys Compd. 352 (2003) 163–167.
[3] C.H. Jung, S.J. Lee, Int. J. Refract. Met. Hard Mater. 23 (2005) 171–173.
[4] J. Sun, C. Liu, R. Wang, Mater. Sci. Eng. A 519 (2009) 27–31.
[5] S. Hayun, S. Kalabukhov, V. Ezersky, M.P. Dariel, N. Frage, Ceram. Int. 36 (2010) 451–457.
[6] D.V. Dudina, D.M. Hulbert, D. Jiang, C. Unuvar, S.J. Cytron, A.K. Mukherjee, J. Mater. Sci. 43 (2008) 3569–3576.
[7] F. Zhang, Z.Y. Fu, J.Y. Zhang, H. Wang, W.M. Wang, Y.C. Wang, J. Shi, Mater. Sci. Forum 620–622 (2009) 395–398.
[8] D. Jianxin, A. Xing, J. Mater. Process. Technol. 72 (1997) 249–255.
[9] Y.W. Kim, L.J. Gunn, J. Am. Ceram. Soc. 72 (1989) 1333–1337.
[10] S.G. Huang, K. Vanmeensel, O. Van der Biest, J. Vleugels, Mater. Sci. Eng. A 527 (2009) 584–589.
[11] J.H. Chaea, K.H. Kima, Y.H. Choac, J. Matsushitad, J.W. Yoona, K.B. Shim, J. Alloys Compd. 413 (2006) 259–264.
[12] Y.M. Ko, W.T. Kwon, Y.W. Kim, Ceram. Int. 30 (2004) 2081–2086.
[13] J. Liu, P.D. Ownby, J. Am. Ceram. Soc. 74 (1991) 674–677.
[14] A. Nakahira, K. Niihara, J. Ceram. Soc. Jpn. 100 (1992) 448–453.
[15] J. Pérez-Rigueiro, J.Y. Pastor, J. Llorca, M. Elices, P. Miranzo, J.S. Moya, Acta Mater. 46 (1998) 5399–5411.
[16] D. Sciti, J. Vicens, A. Bellosi, J. Mater. Sci. 37 (2002) 3747–3758.
[17] L.P. Ferroni, G. Pezzotti, J. Am. Ceram. Soc. 85 (2002) 2033–2038.
[18] X. Sun, J.G. Li, S. Guo, Z. Xiu, K. Duan, X.Z. Hu, J. Am. Ceram. Soc. 88 (2005) 1536–1543.
[19] J.H. Chae, K.H. Kim, Y.H. Choa, J. Matsushita, J.W. Yoon, K.B. Shim, J. Alloys Compd. 413 (2006) 259–264.
[20] C.H. Jung, C.H. Kim, J. Mater. Sci. 26 (1991) 5037–5040.
[21] Z. Shen, Z. Zhao, H. Peng, M. Nygren, Nature 417 (2002) 266–269.
[22] Z.A. Munir, U. Anselmi-Tamburini, M. Ohyanagi, J. Mater. Sci. 41 (2006) 763–777.
[23] J.R. Groza, A. Zavaliangos, Mater. Sci. Eng. A 287 (2000) 171–177.
[24] D.S. Perera, M. Tokita, S. Moricca, J. Eur. Ceram. Soc. 18 (1998) 401–404.
[25] K. Vanmeensel, A. Laptev, J. Hennicke, J. Vleugels, O. Van der Biest, Acta Mater. 53 (2005) 4379–4388.
[26] K. Vanmeensel, A. Laptev, O. Van der Biest, J. Vleugels, Acta Mater. 55 (2007) 1801–1811.
[27] Image-Pro Plus, Version 4, Media Cybernetics, Silver Spring, Maryland, 1999.
[28] D.K. Shetty, I.G. Wright, P.N. Mincer, A.H. Clauer, J. Mater. Sci. 20 (1985) 1873–1882.
[29] K. Niihara, J. Mater. Sci. Lett. 2 (1983) 221–223.
[30] L. Wang, Z.A. Munir, J.B. Holt, J. Mater. Synth. Process. 2 (1994) 217–225.
[31] K.V. Logan, J.T. Sparrow, W.J.S. McLemore, in: Z.A. Munir, J.B. Holt (Eds.), Combustion and Plasma Synthesis of High Temperature Materials, VCH Publishers, New York, 1990.
[32] L. Yonghe, Y. Sheng, Z. Weijing, L. Hoyi, Scripta Mater. 39 (1998) 1237–1242.
[33] C.W. Bale, P. Chartrand, S.A. Degterov, G. Eriksson, K. Hack, R.B. Mahfoud, J. Melancon, A.D. Pelton, S. Petersen, Calphad 26 (2002) 189–228.
[34] L.M. Litz, R.A. Mercuri, J. Electrochem. Soc. 110 (1963) 921–925.
[35] Y.Q. Li, T. Qiu, Mater. Sci. Eng. A 444 (2007) 184–191.
[36] V. Swamya, I.H. Jungb, S.A. Decterovc, Int. J. Mater. Res. 98 (2007) 987–994.
[37] A.T. Shonhiwa, Alumina–cubic boron nitride composite materials, Ph.D. Thesis, University of Witwatersrand, Johannesburg, 2008.
[38] S. Palmqvist, Arch. Eisenhuttenwes 33 (1962) 629–633.
[39] S. Hayun, V. Paris, M.P. Dariel, N. Frage, E. Zaretzky, J. Eur. Ceram. Soc. 29 (2009) 3395–3400.
[40] Z. Jihua, Doctoral Dissertation, University of Science and Technology, Beijing, 1995.